Thermoelectric Material Fabrication using Mask Image Projection Based Stereolithography Integrated with Hot Pressing

Lakshya Tiwari[1], Tengteng Tang[1], Jiahui Rong, Weitong Shan, Yang Yang[2] and Xiangjia Li[1,*]

[1]*Department of Aerospace and Mechanical Engineering, School for Engineering of Matter, Transport and Energy, Arizona State University, 501 E. Tyler Mall, Tempe, AZ 85287*

[2]*Department of Mechanical Engineering, College of Engineering, San Diego State University, 5500 Campanile Drive, San Diego, CA 92182-8080*

Abstract: Waste energy harvest using thermoelectric (TE) materials will be a potential solution to the serious environmental pollution and energy shortage problems. Due to limitations of current manufacturing techniques in geometry complexity and high density, TE devices are not widely utilized in daily life to gather waste energy. 3D printing brings an opportunity to solve the fabrication limitations. In this paper, a hybrid process was developed to fabricate thermoelectric materials by integrating hot pressing with stereolithography. The mold and punch were designed and printed to fabricate thermoelectric devices used on hot water tubes via stereolithography. The $Sb2Te_3$ powders filled the 3D printed mold in a layered manner, and each layer of powders was compacted under the pressing of punch at a certain temperature and compressive force. The polymer mold was removed after the sintering process to form the final TE components. A series of experiments were conducted to identify the optimal heating temperature and compressive force. The microstructures morphology and electrical conductivity of fabricated $Sb2Te_3$ samples were evaluated. This research work conducted a scientific investigation into the fabrication of TE material with a hybrid process, including hot pressing and 3D printing, to solve the current manufacturing challenges, providing perspectives on developments of TE devices used in various energy harvest applications.

Keywords: Thermoelectric material, 3D printing, Stereolithography, Hot pressing, Electrical conductivity.

1. INTRODUCTION

1.1. Thermoelectric Material and Application

Thermoelectric (TE) effect describes a phenomenon that an electric potential can be produced due to a temperature difference. These underlying mechanisms are referred to as the Peltier effect (the electric current helps to drive the heat flow) and the Setback effect (where a potential difference results from temperature differences). The TE effect is present in most materials, but it is typically too weak to be useful [1, 2]. Inorganic-polymer TE composites and inorganic-TE materials are the most common types of TE materials [3, 4]. In a TE power generator, the temperature difference between the hot and cold sides, the geometric design of the power generator, and the TE property of the material all have a significant impact on its conversion efficiency [5, 6]. TE materials exhibit an exceptional ability to convert thermal energy directly into electricity, and they are expected to lead to new cooling technologies as well as devices that harvest waste heat for greater energy efficiency. Hence, TE materials have been widely used in the industry, including thermopower systems, microelectronics, optoelectronics, solar cells, high-tech domains, and power production. Power generation is one of the most promising uses of TE materials [7, 8]. Due to the TE generators' outstanding abilities to boost energy system efficiency, researchers are growing interested in applying them to next-generation TE devices [9-11].

1.2. Traditional Manufacturing Technologies of TE Material

TE materials are often manufactured using powder- and crystal-growth-based methods. Powder-based approaches are acceptable to manage and maintain optimal carrier distribution, particle size, and composition [12]. In powder-based processes, TE powders are stacked layer by layer under pressing and different types of TE powders are blended with varying ratios during the pressing [12, 13]. In the crystal melting process, disks of TE materials are stacked on top of one another, and TE components are fused into the final TE device by using a moving heater [13]. Dopants are frequently mixed under melting in crystal development processes, and TE crystals are produced using a flux approach. For example, thin TE films are designed and fabricated for some purposes, such as cooling electronic circuits, and they can be synthesized using physical vapor deposition techniques [12]. Metal-

*Address correspondence to this author at the Department of Aerospace and Mechanical Engineering, School for Engineering of Matter, Transport and Energy, Arizona State University, 501 E. Tyler Mall, Tempe, AZ 85287;
Tel: (480) 727-8612; E-mail: xiangjia.li@asu.edu

E-ISSN: 2410-4701/22

organic chemical vapor deposition is also used to manufacture thin-film TE devices for enhanced material properties. An energy-dispersive X-ray spectrometer and a powder X-ray diffraction apparatus are used to determine the structures and crystal growths of TE material [13]. Current manufacturing technologies of TE materials require a lot of energy and time to produce TE devices and they are very difficult to produce TE devices with complex three-dimensional (3D) shapes and securely bonded final product, resulting in limited energy harvesting applications [14].

1.3. 3D Printing of TE Material

Additive manufacturing (aka 3D printing) is widely used to build a 3D object from a computer aided designed (CAD) digital model by accumulating material in a layer manner. [16] It can be carried out via a variety of techniques such as stereolithography (SLA), selective laser sintering/melting, and direct ink writing (DIW), where the material is solidification by different mechanisms. Due to the low cost and easy operation, DIW offers a timely and economical method for fabricating complicated structures from a wide variety of materials [17]. Applications include the creation of biomedical devices, chemical and physical sensors, and printed flexible electronics [17]. Compared with other 3D printing technologies, the DIW process benefits from its simplicity in handling ceramic and nanocomposite fabrication, and it has received a lot of attention for producing TE materials [17]. With additive binders, the rapid fabrication of TE materials with complex features is possible by using DIW. The DIW-printed TE devices enable absorbing heat while generating electricity. Furthermore, the flexible, high-performing, and solution-printable TE materials can be printed by DIW due to its capability of fitting complicated geometries into small and limited places. Compared to conventional manufacturing methods, 3D printing has the potential to produce TE products with 3D geometries. However, the density of TE products printed by current 3D printing such as DIW is limited to the addition of binders. Moreover, since parts are created via 3D printing layer by layer, the surface quality and homogeneity made significant effects on the physical properties of TE material [17]. Besides, direct 3D printing of TE material also faces many deficiencies that need to be addressed including excellent quality and consistency [5,16].

1.4. Outline and Contribution

With the development of TE generators, lost thermal energy can be recovered, energy can be produced in harsh conditions, electricity can be produced in off-the-grid locations, and microsensors can be powered [8]. Cogeneration power plants generate electricity while also using heat for other reasons. Such systems or the production of solar thermal energy may use TE material. As we would be able to collect waste heat energy from numerous sources and utilize it in the form of electricity to power various equipment or devices, TE materials could be a step towards a sustainable environment [9-11]. TE materials based on bismuth telluride (Bi_2Te_3) are most frequently employed to develop energy harvest devices [3, 4]. TE-made devices have lots of advantages such as compact size, lack of gas emissions, and great stability [4]. However, the poor conversion efficiency of 3D printed TE components caused by low density and large porosity is the main barrier preventing TE power generators and coolers from being used widely [4]. It is desired to investigate new manufacturing process of TE material with complex geometries for future application. In this paper, we developed a new hybrid fabrication method of TE material with low resistance by utilizing 3D printing and hot pressing. SLA was used to print mold and pressing punch to fabricate TE generator for energy harvesting. Sb_2Te_3 powders were filled into the 3D printed mold layer by layer and compressed at a certain temperature with constant forces. We designed the experiments and studied the effect of fabrication parameters including heat treatment temperature, compressive force, and post sintering on properties of the formed Sb_2Te_3 samples. The micromorphology and electrical conductivity of Sb_2Te_3 samples with and without sintering were evaluated.

2. HYBRID PROCESS DEVELOPMENT

2.1. Material Preparation

For the creation of the energy harvesting device, Sb_2Te_3 material was used to demonstrate the fabrication capability of our new process. The Sb_2Te_3 material bar was chopped into little pieces to assist in the grinding. To enable filling the mold, the little pieces were weighed and ground into microscale powders. The powdered Sb_2Te_3 particles are subsequently filtered through two meshes of 200 μm and 100 μm one after the other. This provides us with powdered Sb_2Te_3 particles that are less than 100 μm. This contributed to enhanced product quality, shape, and cost-effectiveness as well as part uniformity.

2.2. Mold and Punch Fabrication vis SLA

The TE generator can be developed to harvest the energy from hot waste water in the industry (refer to

Figure **1a**). The punch is essentially designed to compress Sb_2Te_3 powders inside the mold so that there are no obvious gaps between particles even without the addition of binders. The digital 3D models of the mold and relevant punch were designed based on the desired shape of the Sb_2Te_3 component (refer to Figure **1b**). Both the mold and punch were printed by using low-cost commercial liquid-crystal display (LCD) based SLA (a Sonic Mini 4K printer). The schematic diagram of LCD-SLA 3D printer is shown in Figure **1c**, and Aqua gray 4K resin was used to produce the mold and the punch. The digital information of the CAD model was uploaded to the printer and the CAD model was sliced into a series of mask images with a layer thickness of 100 µm as shown in Figure **1b**. The LCD screen and UV light source are the projection unit's essential parts, and LCD screen serves the purpose of displaying projection light beam using different mask images [18, 19]. When the mask image is projected on the screen, it solidifies the area that is illuminated into the desired shape. The resin vat is filled with Aqua gray 4K resin and the build platform completely submerge. The model builds on the platform and the platform moves up after each layer's fabrication. Additionally, the layer thickness of the software-sliced CAD model determines the total layer numbers of fabrication and the printing surface quality [20]. The printing steps described here are used to create both the mold and the punch, and the overall fabrication process takes 20 mins.

2.3. Hot Pressing Integration

The Sb_2Te_3 green part can be formed using the high-force, low-strain-rate hot pressing at a high temperature to trigger the creep process, leading to low porosity and high density. An illustration of the hot pressing of Sb_2Te_3 powders into desired 3D shape with the help of 3D printed mold is shown in Figure **2**. Specifically, the SLA-printed punch is attached to the up-temperature-controllable plate, and the SLA-printed mold is placed between the up and down temperature-controllable plates. Layers of powdered Sb_2Te_3 material were filled inside the mold and further were pressed by the SLA-printed punch at a certain temperature (100 °C and 200 °C) and compressive force (500 N and 1000 N). The built-in temperature sensor was used to monitor the temperature and an Arduino-based basic force sensor was used to monitor the compressive force. A lever built into the hot pressing homemade set-up was used to provide the force to accommodate the movement of one of the heating plates. Sb_2Te_3 powders congregated in areas of tension while decreasing in areas of compression, and a new layer of Sb_2Te_3 powders was filled to fabricate the next layer and the above steps were repeated until the pressed Sb_2Te_3 powder filled up the SLA printed mold. Different temperatures and forces were tested during the hot pressing procedure. The integration of hot pressing aids in the removing of air space between Sb_2Te_3 powders and converting into a solid form.

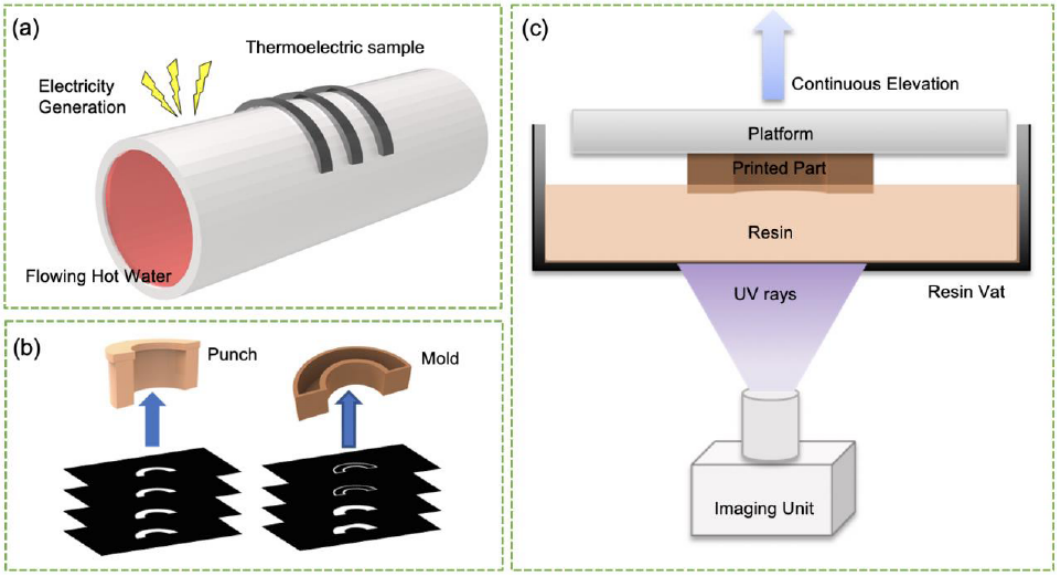

Figure 1: A schematic illustration of design process of mold and relevant punch for TE pipe fabrication using LCD-SLA (**a**) Thermoelectric pipe design for the electricity generation; (**b**) projection mask images generation for the formation of mold and punch; and (**c**) schematic diagram of the printing process.

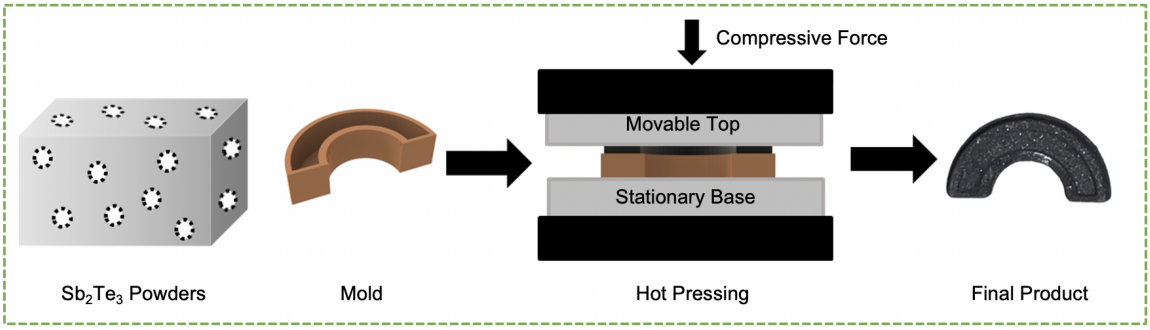

Figure 2: A schematic illustration of the hot pressing of Sb_2Te_3 powders with assistance of SLA printed mold and punch.

2.4. Sintering and Thermogravimetric Analysis

Sb_2Te_3 powders are sparsely arranged and an additional sintering process is necessary to fuse the Sb_2Te_3 powders and remove the SLA printed mold [20]. Hence, the printed Sb_2Te_3 sample obtained by preliminary hot pressing was further sintered in accordance with the temperature changed as shown in Figure **3a**. With a rising temperature under the rate of 2 °C /min, each stage of the sintering process had a dwell time of around 25 minutes to facilitate appropriate diffusion among the fine Sb_2Te_3 particles. The Sb_2Te_3 sample was heated for 250 minutes at the sintering temperature (380 °C), which was reached after 350 minutes of heating. Each hot pressing formed Sb_2Te_3 samples were obtained with the desired shape after sintering. The total time for the sintering process was 995 minutes including the step of cooling to room temperature.

The thermogravimetric analysis (TGA) of cured polymer resin was performed in pinholed aluminum crucibles at a heating rate of 10 °C /min from room temperature 24.25 °C to 700 °C under nitrogen purging (10 mL/min) as shown in Figure **3d**. From the TGA analysis, the polymer printed mold turned to be loose after the sintering process and the geometric shape was maintained since the sintering temperature was lower than the temperature at which the polymer is fully burning out.

2.5. Fabrication Process Planning

The fabrication of Sb_2Te_3 materials entails procedures including 3D printing, material filling, hot pressing, and sintering. The mold and punch were first printed using SLA from the sliced digital models before the hot pressing procedures of the Sb_2Te_3 powders using the photocurable acrylate resin. Isopropyl alcohol was used to remove the residual resin on the SLA-printed mold and punch. Sb_2Te_3 powders were filled with the mold and then pressed into the mold by the printed punch on the hot pressing plate from the top under a certain temperature and compressive force. Using the predefined sintering curve, the hot-pressed Sb_2Te_3 samples were sintered to achieve the best diffusion among Sb_2Te_3 particles. Finally, the Sb_2Te_3 part was removed from the mold for carrying out various performance tests such as microstructure characterizations and electrical conductivity.

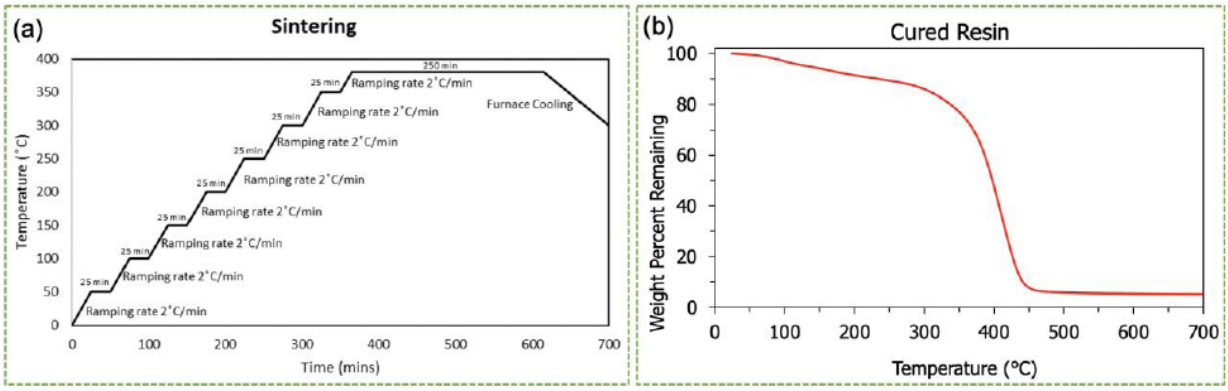

Figure 3: (**a**) Temperature curve for sintering of Sb_2Te_3 samples;(**b**) TGA analysis of SLA printed polymer mold.

2.6. Morphology of Microstructures and Electrical Conductivity

Secondary electron microscope analysis was performed on fabricated samples to evaluate the uniform of microstructures. The resistance of printed samples was measured using an Ossila four-point probe, and then the electrical conductivity of the fabricated Sb_2Te_3 samples was calculated based on the measurements. The statistical analysis theory was applied in the experimental design and analysis in this study. Three samples were measured and all data presented here were with standard deviation (SD).

3. RESULTS AND DISCUSSION

3.1. Process Parameters Optimization

There are several process parameters for the developed fabrication technique being optimized to fabricate Sb_2Te_3 powders with desired density and microstructures' morphology. In terms of hot pressing, heat treatment temperature, compressive force, as well as the holding duration are very crucial to the fabrication of Sb_2Te_3 powders. In this paper, among these three influencing factors, we focused on the study of heat treatment temperature and compressive force regarding the density improvement of Sb_2Te_3 samples and set 5 minutes for holding each sample at certain heating temperature and compressive force. Hence, we designed two factors experiments and each factor has two levels to identify the relation between the fabrication results and main fabrication parameters. Specifically, the samples were created under experimental conditions that involve the pressing temperature of 100 °C or 200 °C in association with a compressive force of 500 N or 1000 N.

Compression and heat treatment are applied in unison to accomplish the creeping deformation. As a primary method of forming, Nabarro-Herring Creep and Coble Creep may take place during such pressing process of Sb_2Te_3 powders. Both types of diffusional creep are extremely sensitive to temperature and force. [18] The experimental results demonstrated that Sb_2Te_3 powders tends to form a solid form due to the diffusion of particles at high compressive force and heating temperature even before the sintering process. Additionally, the surface of the sample tends to have a crystal shine after the hot pressing at 200 °C or 1000 N, which indicates that recrystallization is occurring on the Sb_2Te_3 powders during the hot pressing (Figure **2**). The creeping deformation occurs and affects the diffusion of Sb_2Te_3 powders in the heat treatment and compression. For a higher pressing temperature and compressive force, it is notable that more dense parts can be fabricated, which explains how the resistivity in the experimental measurement can be significantly reduced at larger temperatures and force in session 3.3.

After applying heat treatment and compressive force, sintering was conducted to further compress and solidify Sb_2Te_3 powders before totally melting. We further conducted the experiment to evaluate the effect of the sintering process on the density of printed Sb_2Te_3 samples. The sintered samples were removed from the SLA-printed molds and various tests were carried out to improve the density of Sb_2Te_3 parts. The

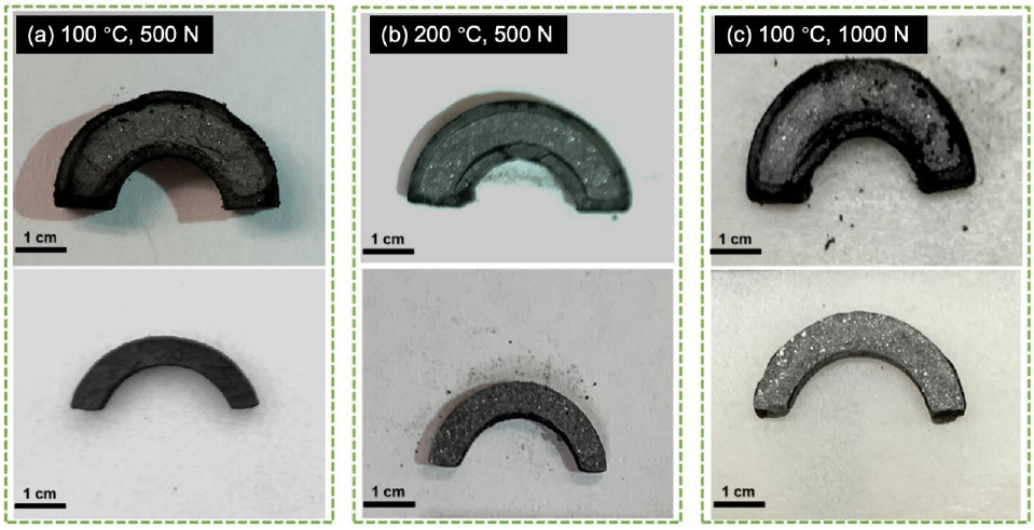

Figure 4: Sample images before and after the removal from the SLA printed molds using the hot pressing at temperatures and compressive forces of (**a**) 100 °C, 500 N; (**b**) 200 °C, 500 N; and (**c**) 100 °C, 1000 N.

image in Figure **4a** shows a sintered sample that was heat-pressed at 100 °C with a compressive force of 500 N. Powdered Sb_2Te_3 particles have been formed into a single sample, but there is not much surface indication of recrystallization due to the low compressive force and heating temperature. When the pressing temperature was increased to 200 °C and kept the compressive force at 500 N, there were metal shining dots on the sample's surface due to the crystallization (refer to Figure **4b**). The greater number of lustrous particles reflects better recrystallization in the sample when the sample was thermally pressed with a force of 1000 N at 100 °C (refer to Figure **4c)**. Along with the creep deformation, recrystallization can be observed on the Sb_2Te_3 sample when compressive force or pressing temperature is raised. Based on the experimental results, the density of the Sb_2Te_3 sample improved higher by increasing the compressive force from 500 N to 1000 N compared with the temperature increasing from 100 °C to 200 °C.

3.2. Microstructures Characterization

The microstructures of fabricated Sb_2Te_3 samples that were hot pressed at different temperatures and compressive forces were examined before and after the sintering processes. We studied the microstructural morphology of Sb_2Te_3 samples fabricated using different parameters through scanning electron microscope (SEM) imaging to figure out the optimal fabrication parameters. The two main factors that affect the density of Sb_2Te_3 samples are heating temperature and compressive force, which are crucial to the integrity of the fabrication process of Sb_2Te_3 material. The creep deformation of Sb_2Te_3 powders packed inside the mold occurs depending on the setting of the heating temperature and compressive force during the hot pressing and the sintering process. As shown in Figure **5a1**-**c1**, there are more porous structures on the surface of non-sintered Sb_2Te_3 sample compared with that of sintered samples. The grain size of Sb_2Te_3 powders increases and the pore size decreases after the sintering process (Figure **5a2**-**c2**). Sb_2Te_3 powders diffuses into a whole part and the bonding between Sb_2Te_3 powders is enhanced after the sintering.

The non-sintered and sintered samples in Figure **5a** and **5b** were fabricated under the compression at a force of 500 N and 1000 N, respectively, while being heated at 100 °C. Samples clearly show that the grain boundary is inappropriately formed and the material's surface is covered in porous structures when the compressive force was set at 500 N. The crystallization only occurred in a small region due to the limited compressive force. The Sb_2Te_3 particles diffused better in the bulk and Sb_2Te_3 microsheets with a larger area

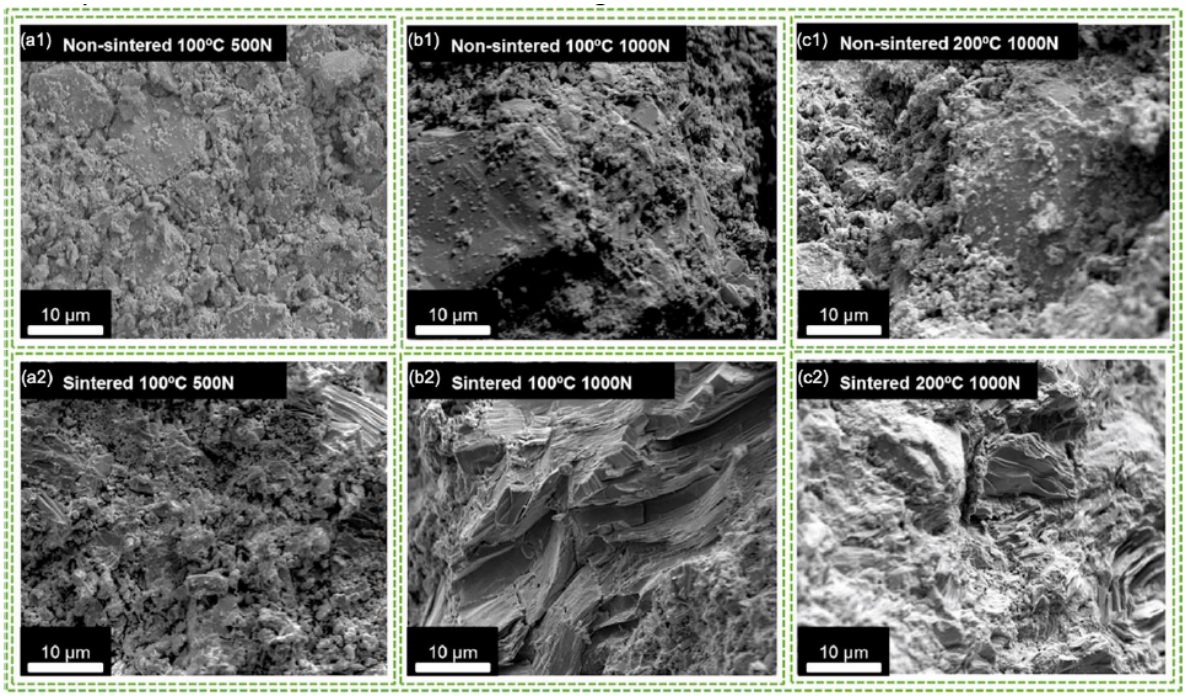

Figure 5: The microstructures morphologies of samples fabricated under the hot pressing temperature and compressive force of (**a**) 100 °C, 500 N; (**b**) 100 °C, 1000 N; (**c**) 200 °C, 500 N; (**d**) 100 °C; 500 N; (**e**) 100 °C, 1000 N; and (**f**) 200 °C, 500 N.

were formed under the 1000 N compressive force (Figure **5b**). Figure **5b** and **5c** show SEM images of samples that were heated at 100 °C and 200 °C, respectively, maintaining compressive force at 1000 N. It is noted that the grain boundary of the one fabricated at 200 °C is much better and more well-constructed than the one at 100 °C. The surface of the sample that was heated at 200 °C exhibits less porous structures with more crystallization during the hot pressing. Based on the SEM images, the Sb_2Te_3 powders created well-constructed grain boundaries and formed crystalline structures in the sintered sample, which were heated to 200 °C and compressed with a force of 1000 N.

3.3. Electrical Conductivity

The electrical conductivity of fabricated Sb_2Te_3 samples determines the efficiency of the further application of waste energy harvest. The electrical conductivity of fabricated Sb_2Te_3 samples was measured and the results are shown in Figure **6**. High density of Sb_2Te_3 components results in low resistance. Sintering reduced the quantity and size of holes that were present between Sb_2Te_3 particles so that sintered samples had lower electrical resistivity than non-sintered samples. Most of Sb_2Te_3 particles crept under the 1000 N compressive force, and the sintering appeared ineffective in further reducing the porosity and improving the density. The difference between the sintered and non-sintered samples fabricated under 1000 N is only 0.4 $\Omega \cdot mm$.

Figure **6a** shows the relationship between the resistivity and the compressive force applied during hot pressing for sintered and non-sintered samples. The result shows that Sb_2Te_3 samples increasingly densify by applying higher compressive force. When the compressive force reached 1000 N, the resistivity of non-sintered Sb_2Te_3 samples reduced dramatically from 18.7 $\Omega \cdot mm$ to 8.6 $\Omega \cdot mm$. After the sintering, the resistivities of Sb_2Te_3 samples hot pressed under 500 N and 1000 N are similar when the pressing temperature is 100 °C. Temperature played a significant role in improving the density and reducing the resistivity. The relationship between resistivity and pressing temperature is shown in Figure **6b**. The sintered sample that is pressed at a higher temperature display a lower resistivity than other samples. Sb_2Te_3 powder crystallization is aided by higher pressing temperatures. Meanwhile, the resistivity between the sintered and non-sintered samples differ significantly when the compressive force was 500 N.

4. CONCLUSION AND FUTURE WORK

Here we developed a novel hybrid process by using SLA and hot pressing to achieve high density and electrical conductivity. SLA was used to fabricate complement molds and punches for the formation of the 3D shape of Sb_2Te_3 in the following processes. The SLA-printed mold was filled with Sb_2Te_3 powders layer by layer. Each layer of Sb_2Te_3 powders received consistent compressive force and heat treatment for 5 mins to induce the creep. The densification of Sb_2Te_3

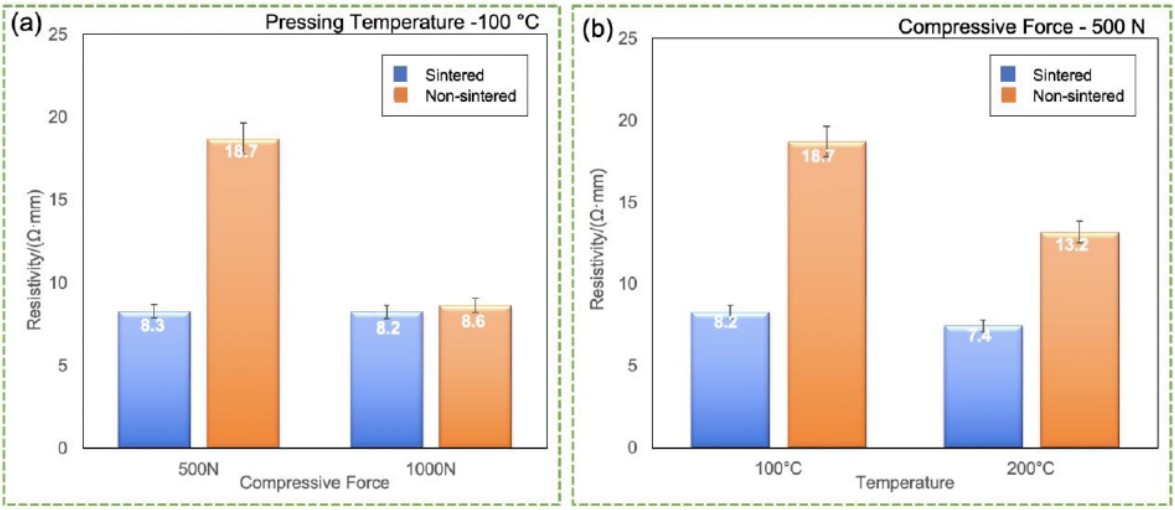

Figure 6: Resistivity in relation to compressive force and pressing temperature. (**a**) the relationship between resistivity and compressive force under the sintered and non-sintered condition; and (**b**) the relationship between resistivity and pressing temperature under the sintered and non-sintered condition.

powders was achieved through hot pressing at 200 °C below the melting temperature of the printed polymer mold. The heat treatment as well as a compressive force both played major roles in controlling the morphology and property of printed Sb_2Te_3 samples. The variation of material characteristics on heat treatment temperature and compressive force was studied. To get the optimum morphology of micro/nanostructures, sintering process was conducted after the printing to further condense and enhance the properties of the Sb_2Te_3 samples. After the sintering, the polymer-based mold was loose and the printed Sb_2Te_3 samples were removed from the mold. To optimize the fabrication parameters, several specimens were made to examine electrical conductivity without/with the sintering, which shows how sintered and non-sintered samples differ in the performance of electrical conductivity. Due to the integration of hot pressing and SLA, the printed Sb_2Te_3 samples show improvement in compactness and density. Experiments conducted on test cases demonstrated that the presented process reached 7.4 $\Omega \cdot \mathrm{mm}$. Our method solves the current challenges in the fabrication of TE materials with complex geometry by integrating hot pressing with 3D printing, and the density of printed parts was dramality improved, which would enable the effectiveness of waste energy harvesting. In the future, we will further test energy harvesting properties of fabricated Sb_2Te_3 components. The efficiency of other types of TE materials will be also studied using our developed method.

ACKNOWLEDGEMENT

The authors acknowledge ASU startup funding, ASU FSE Strategic Interest Seed Funding, National Science Foundation (NSF Grant No. CMMI-2114119). The authors also thank the ASU core research facilities for the use of SEM electron microprobe analyzer, and Prof. Kailong Jin's Lab for the test of the TGA.

REFERENCES

[1] Goldsmid HJ. Review of thermoelectric materials. Introduction to Thermoelectricity 2016 (pp. 153-195). Springer, Berlin, Heidelberg. https://doi.org/10.1007/978-3-662-49256-7_9

[2] Snyder GJ, Toberer ES. Complex thermoelectric materials. In Materials for sustainable energy: a collection of peer-reviewed research and review articles from Nature Publishing Group 2011 (pp. 105-114). https://doi.org/10.1142/9789814317665_0016

[3] Sootsman JR, Chung DY, Kanatzidis MG. New and old concepts in thermoelectric materials. Angewandte Chemie International Edition. 2009 Nov 2; 48(46): 8616-39. https://doi.org/10.1002/anie.200900598

[4] Liu W, Hu J, Zhang S, Deng M, Han CG, Liu Y. New trends, strategies and opportunities in thermoelectric materials: a perspective. Materials Today Physics. 2017 Jun 1; 1: 50-60. https://doi.org/10.1016/j.mtphys.2017.06.001

[5] Orrill M, LeBlanc S. Printed thermoelectric materials and devices: Fabrication techniques, advantages, and challenges. Journal of Applied Polymer Science. 2017 Jan 15; 134(3). https://doi.org/10.1002/app.44256

[6] Snyder GJ, Snyder AH. Figure of merit ZT of a thermoelectric device defined from materials properties. Energy & Environmental Science. 2017; 10(11): 2280-3. https://doi.org/10.1039/C7EE02007D

[7] Snyder GJ. Energy Harvesting Technologies ed S Priya and DJ Inman.

[8] Zhao D, Tan G. A review of thermoelectric cooling: materials, modeling and applications. Applied thermal engineering. 2014 May 1; 66(1-2): 15-24. https://doi.org/10.1016/j.applthermaleng.2014.01.074

[9] Molina-Lopez F. Emerging thermoelectric generators based on printed and flexible electronics technology. In2020 IEEE SENSORS 2020 Oct 25 (pp. 1-4). IEEE. https://doi.org/10.1109/SENSORS47125.2020.9278922

[10] Shakeel M, Rehman K, Ahmad S, Amin M, Iqbal N, Khan A. A low-cost printed organic thermoelectric generator for low-temperature energy harvesting. Renewable Energy. 2021 Apr 1; 167: 853-60. https://doi.org/10.1016/j.renene.2020.11.158

[11] Chen B. Additive manufacturing of flexible energy harvesting and storage device. Ph. D. Thesis. 2019 Jan 1.

[12] Yazdani S, Pettes MT. Nanoscale self-assembly of thermoelectric materials: A review of chemistry-based approaches. Nanotechnology. 2018 Aug 21; 29(43): 432001. https://doi.org/10.1088/1361-6528/aad673

[13] Kwon SD, Ju BK, Yoon SJ, Kim JS. Fabrication of bismuth telluride-based alloy thin film thermoelectric devices grown by metal organic chemical vapor deposition. Journal of electronic materials. 2009 Jul; 38(7): 920-4. https://doi.org/10.1007/s11664-009-0704-8

[14] Mikami M, Yoshimura M, Mori Y, Sasaki T, Funahashi R, Matsubara I. Crystal growth of thermoelectric material NaxCoO2-δ by a flux method. Japanese journal of applied physics. 2002 Jul 1; 41(7A): L777. https://doi.org/10.1143/JJAP.41.L777

[15] He J, Tritt TM. Advances in thermoelectric materials research: Looking back and moving forward. Science. 2017 Sep 29; 357(6358): eaak9997. https://doi.org/10.1126/science.aak9997

[16] Kim F, Kwon B, Eom Y, Lee JE, Park S, Jo S, Park SH, Kim BS, Im HJ, Lee MH, Min TS. 3D printing of shape-conformable thermoelectric materials using all-inorganic Bi2Te3-based inks. Nature Energy. 2018 Apr; 3(4): 301-9. https://doi.org/10.1038/s41560-017-0071-2

[17] Du Y, Chen J, Meng Q, Dou Y, Xu J, Shen SZ. Thermoelectric materials and devices fabricated by additive manufacturing. Vacuum. 2020 Aug 1; 178: 109384. https://doi.org/10.1016/j.vacuum.2020.109384

[18] Zhu, Y., Joralmon, D., Shan, W., Chen, Y., Rong, J., Zhao, H., Xiao S., Li, X. 3D printing biomimetic materials and structures for biomedical applications [J]. Bio-Design and Manufacturing, 2021, 4(2): 405-428. https://doi.org/10.1007/s42242-020-00117-0

[19] Li X, Chen Y. Vat-Photopolymerization-Based Ceramic Manufacturing [J]. Journal of Materials Engineering and Performance, 2021, 30(7): 4819-4836 https://doi.org/10.1007/s11665-021-05920-z

[20] Li, X., Yuan, Y., Liu, L., Leung, Y. S., Chen, Y., Guo, Y., Chai, Y., Chen, Y. 3D printing of hydroxyapatite/tricalcium phosphate scaffold with hierarchical porous structure for bone regeneration [J]. Bio-Design and Manufacturing, 2020, 3(1): 15-29. https://doi.org/10.1007/s42242-019-00056-5

Received on 22-11-2022 Accepted on 19-12-2022 Published on 30-12-2022

DOI: https://doi.org/10.31875/2410-4701.2022.09.11